Title

Optical property measurements of turbid media in a small-volume cuvette with frequency-domain photon migration.

Journal

Applied Optics, 40(34)

ISSN

0003-6935

Authors

Coquoz, Olivier
Svaasand, Lars O
Tromberg, Bruce J

Publication Date

2001-12-01

DOI

10.1364/ao.40.006281

Optical property measurements of turbid media in a small-volume cuvette with frequency-domain photon migration

Olivier Coquoz, Lars O. Svaasand, and Bruce J. Tromberg

A frequency-domain photon migration (FDPM) technique is developed for quantitative measurement of the absorption and reduced scattering coefficients of highly turbid samples in a small-volume (0.45-ml) reflective cuvette. We present both an analytical model for the FDPM cuvette and its experimental verification, using calibrated phantoms and suspensions of living cells. FDPM model fits to experimental data demonstrate that the reduced scattering (μ_s') and absorption (μ_a) coefficients can be derived with accuracies of 5–10% and 10–15%, respectively. Changing the cuvette wall reflectivity alters the frequency-dependent behavior of photon density waves (PDWs). For highly reflective wall boundaries ($R_{\text{eff}} \geq 90$–95%), PDW confinement leads to substantial enhancement in both amplitude and phase compared with identical samples in infinite media. Results from experiments on microsphere suspensions are compared with predictions from Mie theory to assess the potential of this method to interpret scattering properties in terms of scatterer size and density. Optical property measurements of biological cell suspensions are reported, and the possibility of optically monitoring cell physiology in a carefully controlled environment is demonstrated.

OCIS codes: 290.4020, 290.7050, 170.5270, 170.5280, 170.6510, 290.0290.

1. Introduction

A variety of methods have been developed to quantify optical absorption and scattering properties in turbid biological materials.[1] Experimental approaches involve light transmission and reflection measurements by use of integrating sphere,[2–5] temporal dispersion,[6,7] and spatially dependent attenuation[8–10] techniques. In general, all methods compare optical data with a specific governing model for light propagation to calculate absorption (μ_a) and reduced scattering (μ_s') coefficients.

Temporal dispersion techniques can be adapted to amplitude-modulated light sources and phase-sensitive detection. The resulting frequency-domain photon migration (FDPM) methods provide an experimentally simple approach to quantify tissue optical properties.[11,12] In FDPM, the intensity of light incident on a turbid biological material is modulated at high frequencies. Intensity-modulated light propagates through multiple-scattering media with a coherent front, forming photon density waves (PDWs).[13,14] PDW dispersion is highly dependent on optical properties. Thus measurements of the frequency- or distance-dependent PDW behavior can be used to calculate the reduced scattering coefficient μ_s' and absorption coefficient μ_a. To achieve this, analytical expressions provided by a theoretical model describing PDW propagation are fit to the measured PDW phase and amplitude. A model commonly used is based on the diffusion approximation of the Boltzmann transport theory, described by the standard diffusion equation. There are basically two ways that one can perform FDPM measurements: either by varying the source–detector distance while modulating the light at a fixed modulation frequency[14] or by keeping the source and detector at fixed positions and sweeping over a range of frequencies.[13,15,16] In our experiments, the source–detector separation was kept constant during the measurement session while radio-frequency (rf) modulation was swept up to 1 GHz.

FDPM techniques developed so far typically rely on

When this research was performed, the authors were all with the Beckman Laser Institute and Medical Clinic, University of California, Irvine, 1002 Health Sciences Road East, Irvine, California 92612. O. Coquoz is now with Xenogen Corporation, Alameda, California 94501. L. O. Svaasand is also with the University of Trondheim, 7000 Trondheim, Norway. B. J. Tromberg's e-mail address is tromberg@bli.uci.edu.

Received 2 January 2001; revised manuscript received 7 August 2001.

0003-6935/01/346281-11$15.00/0

models that assume either an infinite[13] or a semi-infinite geometry.[17] We have developed a theoretical model for a spherical-boundary geometry to meet the need of interpreting optical property measurements of small-volume samples. Our objective is to perform optical property measurements of tissue biopsies, cell suspensions, or turbid fluids (e.g., blood samples, chemical processes) in a simple geometry.

The spherical geometry was chosen because of its high symmetry, leading to a relatively straightforward analytical model for PDW propagation. A small-volume (0.45-ml) cuvette was constructed to verify experimentally the analytical model. When a highly reflecting material is used to build the chamber, the photon path length is enhanced because of multiple reflections at the wall. In this way, it is possible to increase an intrinsically small phase shift or demodulation signal to a detectable level, thus enhancing the sensitivity of our method to small concentrations of chromophores.

Measurements were performed on scattering liquid samples, namely, solutions of Intralipid (IL), to simulate scattering media with the addition of an absorbing dye [nickel(II) phthalocyanine NiSPC]. We obtained the optical properties by fitting model functions describing the frequency dependence of PDW phase and amplitude to the actual data recorded during the experiments. The capability to derive both absorption and reduced scattering coefficients of small-volume samples uniquely from a single near-real-time measurement is demonstrated.

Among the possibilities offered by the FDPM cuvette is the ability to perform experiments on small, well-defined volumes of material (0.45 ml). These experiments are of interest to build a base of knowledge to interpret the physical meaning of the transport scattering coefficient. Results of measurements on suspensions of microspheres of different sizes, concentrations, and mixed samples are presented. The measured optical properties are compared with Mie theory, and the accuracy of our technique is discussed.

A set of experiments on cell suspensions was also designed to establish the physiological basis for the interpretation of the optical properties of biological material. Small-volume FDPM experiments on suspensions of human breast carcinoma cells (MCF7) are reported under isotonic and hypertonic conditions for three optical wavelengths.

2. Material and Method

A. Diffusion Theory in the Frequency Domain

To obtain analytical solutions for the propagation of PDWs in a spherical geometry, we must solve the Boltzmann transport theory with the appropriate boundary conditions corresponding to the sample geometry. In tissue optics, the model usually taken into consideration to evaluate light propagation is based on the diffusion approximation, stating that scattering is the predominant phenomenon occurring in biological tissues, as compared with absorption (i.e., reduced scattering coefficient $\mu_s' \gg$ absorption coefficient μ_a). This statement is valid for wavelengths in the red and near-infrared part of the spectrum. Within this approximation, the radiance L can be expressed by a series of expansion, from which only the zeroth- and first-order terms are taken into account:

$$L = \frac{\varphi}{4\pi} + \frac{3}{4\pi}\,\mathbf{j}\cdot\mathbf{l} + \ldots, \tag{1}$$

where φ and $\mathbf{j}$ are, respectively, the fluence rate and the diffuse photon flux vector. The first term corresponds to an isotropic radiance, and the second term represents an anisotropic term in the direction given by the unit directional vector $\mathbf{l}$. The diffuse photon flux vector $\mathbf{j}$ is given by

$$\mathbf{j} = -D\nabla\varphi, \tag{2}$$

where D, the diffusion constant, is defined by

$$D = \frac{1}{3(\mu_a + \mu_s')}. \tag{3}$$

The optical fluence rate then satisfies a diffusion equation of the following form, called standard diffusion equation:

$$\frac{1}{c}\frac{\partial\varphi(\mathbf{r}, t)}{\partial t} - D\nabla^2\varphi(\mathbf{r}, t) + \mu_a\varphi(\mathbf{r}, t) = S(\mathbf{r}, t), \tag{4}$$

where S is the diffuse photon source density and c is the velocity of light in the medium.

When the scattering medium is assumed to be of infinite extent, and for a sinusoidally modulated source $S \propto \exp(i\omega t)$, the general solution of Eq. (4) for the fluence rate is expressed in the form[13]

$$\varphi \propto \exp(-kr)\,\exp(i\omega t), \tag{5}$$

where r is the distance from the source; $\omega = 2\pi f$, where f is the modulation frequency; and k is the complex wave number given by $k = k_{\text{real}} + ik_{\text{imag}}$:

$$k_{\text{real}} = \left(\frac{3}{2}\,\mu_a\mu_s'\right)^{1/2}\left\{\left[1 + \left(\frac{\omega}{c\mu_a}\right)^2\right]^{1/2} + 1\right\}^{1/2}, \tag{6}$$

$$k_{\text{imag}} = \left(\frac{3}{2}\,\mu_a\mu_s'\right)^{1/2}\left\{\left[1 + \left(\frac{\omega}{c\mu_a}\right)^2\right]^{1/2} - 1\right\}^{1/2}. \tag{7}$$

We can derive from these expressions all the parameters defining the PDW propagation, namely, the two parameters coming out of the measurements, i.e., the phase shift Φ and the ac amplitude A, given by

$$\Phi = k_{\text{imag}}\,r, \tag{8}$$

$$A = \frac{1}{4\pi D}\,\frac{\exp(-k_{\text{real}}r)}{r}. \tag{9}$$

B. Photon Density Waves in a Spherical Metallic Cuvette

In the setup considered here, the arrangement is composed of a scattering medium (the actual sample)

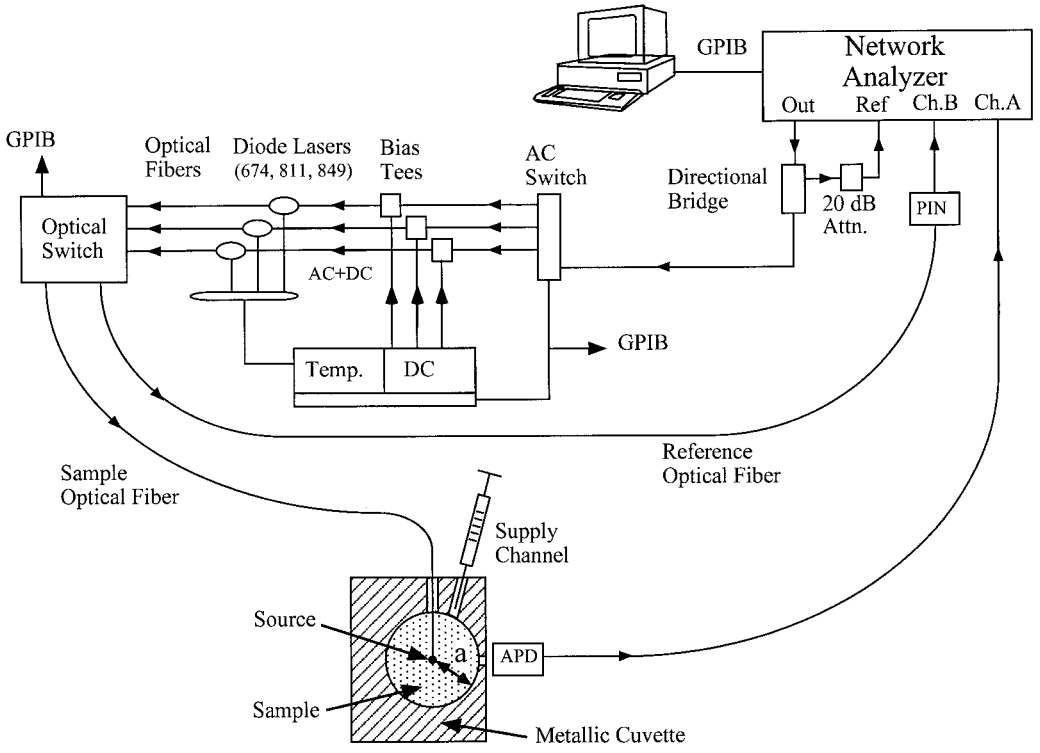

Fig. 1. Schematic diagram of the spherical chamber experimental setup with the FDPM portable device. The network analyzer produces a rf modulation sweep, which is superimposed to the dc bias through a bias tee, to modulate the current driving the laser diodes. The rf and optical switches enable one to select laser diodes of different wavelengths. The light is coupled into an optical fiber, which illuminates isotropically the sample at its center. The radius of the metallic spherical cavity containing the sample is 4.76 mm. The detection is performed by an avalanche photodiode (APD). The signal measured is fed into the network analyzer, where it is compared with a reference signal from a dedicated channel of the optical switch to extract the two desired quantities, phase shift Φ and modulation amplitude A. This experimental setup is remote driven by a computer (Macintosh equipped with LabVIEW, National Instruments Inc.).

confined in the spherical cavity of a metallic container (Fig. 1). The refractive index of metals contains an imaginary part, which is responsible for partial absorption of light within its first superficial atomic layers. To take into account this light loss in our model, we assume that the imperfect reflectivity of the metal acts as if the boundary between the sample and the metal behaves as a radiative-type boundary. In other words, we consider the absorption of photons at the metallic wall as equivalent to the loss of photons at a radiative boundary (i.e., boundary with air).

The source is set at the center of the sphere. The fluence rate in the scattering medium is in this case defined by the sum of forward- and backward-propagating terms:

$$\varphi = \frac{B_1}{r}\exp(-kr) + \frac{B_2}{r}\exp(kr), \qquad r < a. \quad (10)$$

The coefficients B_1 and B_2 are determined by the boundary and initial conditions. The initial condition states that the total radial flux at the origin is equal to the power of the source:

$$P = \lim_{r\to 0} 4\pi r^2 j. \quad (11)$$

The radiative boundary condition implies that the irradiance at the boundary is set equal to the reflected radiance at the interface between a diffusive and a nondiffusive medium, in this case at the surface of the sphere (i.e., at $r = a$, where a is the sphere radius), and can be approximated as

$$\varphi|_{r=a} = \Omega j|_{r=a}, \quad (12)$$

where, for a spherical geometry, j is the radial component of the flux vector and Ω is defined as

$$\Omega = 2\,\frac{1 + R_{\text{eff}}}{1 - R_{\text{eff}}}. \quad (13)$$

For a radiative boundary, R_{eff} is the effective reflection coefficient as defined by Haskell *et al.*,[17] which depends on the refractive-index mismatch at the interface. In our case, we set this coefficient R_{eff} as the diffuse reflectance of the metal (i.e., silver-coated aluminum) and made further adjustments to take into account the losses that are due to holes in the cuvette wall (source, detection, and supply channels). We further note that, if the metal was perfectly reflective, R_{eff} would be equal to 1 and Ω would go to infinity. In that ideal case, $j = 0$ at the cuvette boundary, as expected.

With the help of Eqs. (10)–(13), we can derive the

frequency dependence of both phase and ac amplitude, which are the two measured parameters. To obtain the optical properties from measurements, we perform a nonlinear fit of the experimental data, i.e., phase shift Φ and amplitude A, with analytical expressions derived directly from the mathematical expression of the fluence rate:

$$\varphi = \frac{P\{(a - \Omega D)\sinh[k(a - r)] + \Omega Dka\ \cosh[k(a - r)]\}}{4\pi Dr[(a - \Omega D)\sinh(ka) + \Omega Dka\ \cosh(ka)]}, \tag{14}$$

$$\Phi = \arctan\left[\frac{\mathrm{Im}(\varphi)}{\mathrm{Re}(\varphi)}\right], \tag{15}$$

$$A = |\varphi|. \tag{16}$$

C. Experiments

1. Experimental Setup

The setup used for our experiments (Fig. 1) involves a portable high-bandwidth FDPM instrument, the principle of which has been described in previous publications.[18,19] It is based on use of direct amplitude-modulated laser diodes as sources and an avalanche photodiode (APD) as the detector. A network analyzer (Hewlett-Packard Model 8753C), which measures reflection and transmission characteristics of devices and networks, is used here to produce a rf signal swept from 20 MHz to 1 GHz superimposed on the dc of the three laser diodes (SDL, Inc., Models 7421, 5420, and 5421 at 674, 811, and 849 nm, respectively). Each source is addressed serially through a rf switch, and source selection is accomplished by use of an optical switch (DiCon Fiberoptics, Inc., Model GP700). At the optical switch output, light is launched onto a 200-μm optical fiber terminated by a diffuse sphere (PDT Systems, Inc., Model 2808-A03) to ensure an isotropic illumination within the sample. The optical power coupled into the sample ranges from approximately 10 to 30 mW. The tip of the source fiber is positioned at the center of the spherical cuvette. Detection is performed by an APD (Hamamatsu Model C5658) through a thin glass window (0.15 mm thick) placed on the sphere wall. The time required to perform a measurement depends on the precision required to tune to each frequency [characterized by the intermediate-frequency bandwidth], the number of sweeps performed, and the total number of points acquired. For all the measurements reported, we recorded 201 frequency points per sweep. Typically, the acquisition time is 45 s when five frequency sweeps from 20 MHz to 1 GHz are taken at each of three wavelengths and the intermediate-frequency bandwidth is set to 3000 Hz. The network analyzer, rf, and optical switches are driven by a microcomputer and a customized code (LabVIEW, National Instruments). Communication between the computer and the devices is achieved through general-purpose interface bus (GPIB) protocols.

2. Procedure to Extract the Optical Properties

Experimental curves of phase and amplitude versus frequency were fit by use of analytical expressions describing phase and modulation amplitude derived from Eqs. (15) and (16). We performed simultaneous fits to both phase and amplitude using a Levenberg–Marquardt algorithm (*Numerical Recipes in C*[20]) modified by the authors.

Any given phase and amplitude measurement contains contributions from both the sample and the instrument. Therefore a calibration procedure is necessary to subtract the instrument phase component and source amplitude. Then the measurement of the sample response is isolated and independent of the source power [i.e., P in Eq. (14)].[19] To achieve this, at the beginning of each measurement session, we record FDPM data on a phantom with known optical properties. In all the experiments described here, the reference phantom was a solution of IL 2%, the properties of which were derived *a priori* from FDPM measurements performed in infinite-medium geometry.

Our estimation of the value for the effective reflection coefficient of the metallic cuvette wall was based on the specification provided by the company completing the silver-coating deposition (QSP Optical Technology Inc., Santa Ana, Calif.: $R > 95\%$ for $\lambda = 600–1000$ nm). To quantitatively account for the losses that are due to the three channels (source, detection, and supply channels), this coefficient R_{eff} was calibrated at each wavelength, and the resulting values ($R_{\mathrm{eff}} \cong 0.9$ for all three wavelengths) were introduced as a fixed parameter in the sample data processing. The reduced scattering and absorption coefficients were obtained from a nonlinear, simultaneous fit to experimental phase and relative amplitude data.

3. Liquid Phantom Experiments

Experiments were performed on liquid phantoms to assess the ability of our method to derive optical properties from the small spherical cuvette measurements. The frequency dependence of the phase shift and ac amplitude were recorded for solutions containing IL (Pharmacia, Inc., Clayton, Ill.) to simulate scatterers and NiSPC [nickel(II) phthalocyanine, tetrasulfonate, Na, Mid-Century Chemicals, Posen, Ill.) as an absorber at different concentrations, i.e., for different scattering and absorption coefficients. The phantom optical properties were measured in infinite-medium conditions, and we quantified the extinction coefficient of the dye using a spectrophotometer (Beckman Instruments Model DU-7). The results obtained were considered the standard values for the cuvette experiments.

4. Microsphere Experiments

Optical property measurements were recorded on polystyrene microsphere suspensions (Polysciences,

Inc., Warrington, Pa.) of 0.698 μm (2.69% solid fraction), 1.072 μm (2.68%), 1.531 μm (2.61%), and 2.092 μm (2.61%) in diameter. Additional samples included 2.092-μm beads, 1.3% solution, and two mixed samples: mix 1 contained 1.072- and 2.092-μm beads in the ratio 2:1 (1.79% and 0.87% solid fraction, respectively); and mix 2 contained 0.698- and 1.531-μm beads in the ratio 2:1 (1.79% and 0.87% solid fraction, respectively).

We computed Mie predictions using a numerical code modified from Bohren and Huffman,[21] and we derived the reduced scattering coefficient μ_s' using the expression

$$\mu_s' = N\sigma_s' = \frac{\phi}{(4/3)\,\pi a^3}\,\sigma_s(1-g) = \frac{3\phi_s}{4\rho a}\,Q_{\text{scat}}(1-g), \tag{17}$$

where N is the scatterer density (number of scatterers per volume), $\sigma_s(\sigma_s')$ is the (reduced) scattering cross section of an individual scatterer, $\phi(\phi_s)$ is the volume (solid) fraction, ρ is the density of polystyrene ($\rho = 1.05$), and a is the bead radius. The effective scattering parameter Q_{scat} and anisotropy factor g are derived directly from the Mie code and are functions of two parameters: the size factor $x = 2\pi a n_{\text{out}}/\lambda$ and the refractive-index ratio $m = n_{\text{in}}/n_{\text{out}}$, where n_{in} is the polystyrene refractive index ($n_{\text{in}} = 1.59$), n_{out} is the refractive index of the surrounding medium (in our case, $n_{\text{out}} = n_{\text{water}} = 1.33$), and λ is the light wavelength in vacuum.

The reduced scattering coefficient of a mixture of various-sized scatterers is obtained in the following way[22,23]:

$$\mu_{s\,\text{mix}}' = \mu_{s\,\text{mix}}(1-g_{\text{mix}}), \tag{18}$$

where

$$\mu_{s\,\text{mix}} = \sum_i \mu_{si}, \qquad g_{\text{mix}} = \frac{\sum_i \mu_{si} g_i}{\sum_i \mu_{si}}. \tag{19}$$

Although the phase function of a mixture is not of the same type as its individual parts,[22] both the scattering coefficient μ_s and the anisotropy factor g have been shown to be linear combinations of each component.[22,23] Therefore the reduced scattering coefficient μ_s' must also be a linear combination of components. For a two-component system, the reduced scattering coefficient is

$$\begin{aligned}\mu_{s\,\text{mix}}' &= (\mu_{s1}+\mu_{s2})\left(1-\frac{\mu_{s1}g_1+\mu_{s2}g_2}{\mu_{s1}+\mu_{s2}}\right)\\ &= \mu_{s1}+\mu_{s2}-\mu_{s1}g_1-\mu_{s2}g_2\\ &= \mu_{s}'_1+\mu_{s}'_2.\end{aligned} \tag{20}$$

In our experiments we computed the reduced scattering coefficient of the mixture of two different size microspheres by adding the individual reduced scattering coefficients of the two components, taking into account their respective concentration in the mixed solution.

5. *Cell Experiments*

We subcultured human breast carcinoma cells MCF7 in T-25 flasks using fetal bovine serum-supplemented growth media at 37 °C and 7.5% CO_2, as per standard protocols. One week prior to measurements, cells were subcultured into several separate Nunclon triple flasks (Nalge Nunc Int., Naperville, Ill.) and grown to confluence. Cells numbered from 0.5–1.5×10^8 for each experiment and were treated with trypsin–ethylenediaminetetraacetic acid before centrifugation to prevent excessive cell aggregation. Cells were resuspended in small volumes of 1× phosphate-buffered saline without calcium salts at 37 °C to maintain a single-cell suspension for injection into the cuvette. Cell viability in phosphate-buffered saline averages 1–2 h, a period that is adequate because a set of several FDPM measurements requires only a few minutes.

Inert particles, i.e., polystyrene microspheres, were added to the cell suspension to bring the scattering properties to a level ensuring the diffusion regime. The criterion chosen imposes that the distance between the source and the detector is at least five

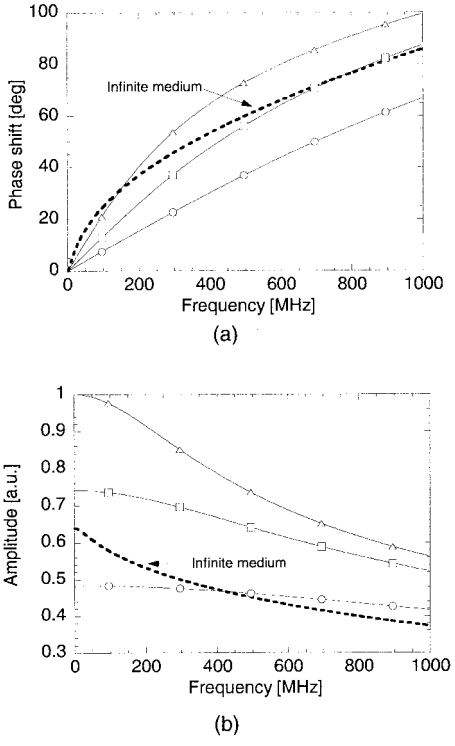

Fig. 2. Model functions for (a) phase shift versus frequency and (b) amplitude versus frequency in a comparison of PDWs in infinite-medium geometry (dashed curves) and in the small spherical cuvette featuring three different values for the effective reflection coefficient $R_{\text{eff}} = 0.95$, 0.9, and 0.75 (solid curves with triangles, squares, and circles, respectively). The sample considered is IL 2% at 670 nm ($\mu_s' = 2.42\ \text{mm}^{-1}$ and $\mu_a = 0.42 \times 10^{-3}\ \text{mm}^{-1}$).

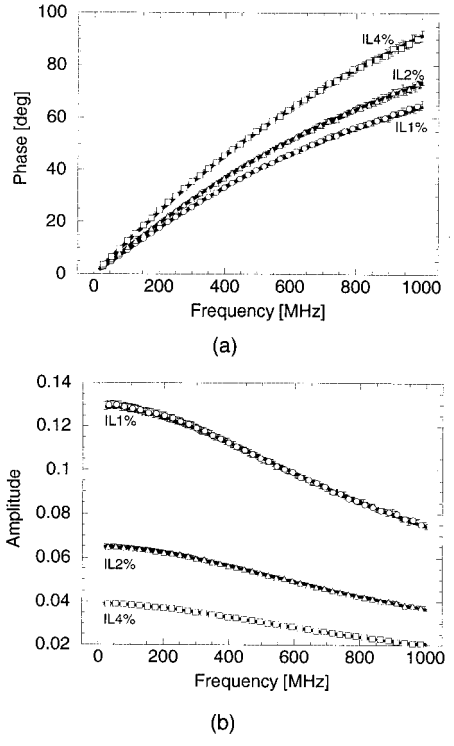

Fig. 3. (a) Experimental phase shift and (b) amplitude data recorded on IL solutions in different concentrations (1%, 2%, and 4%), with no absorber added, in the small-volume cuvette at 849 nm. Model functions resulting from the simultaneous phase and amplitude fit are displayed as solid curves.

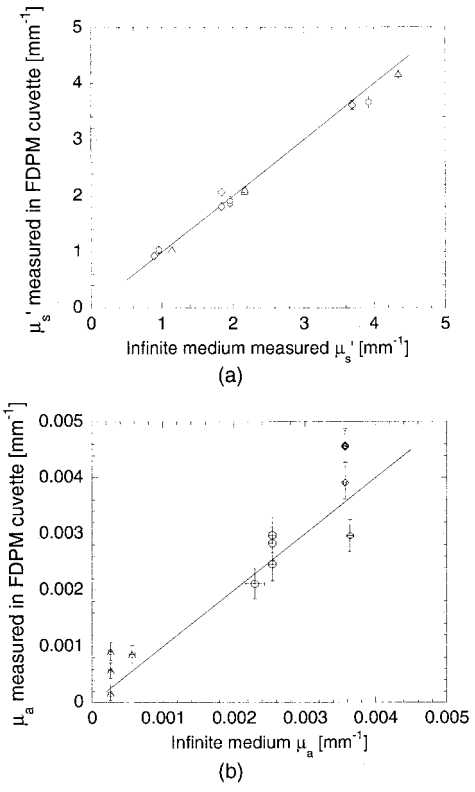

Fig. 4. (a) Reduced scattering coefficients of IL solutions in different concentrations (1%, 2%, and 4%) at 674 nm (triangles), 811 nm (circles), and 849 nm (diamonds) measured in the 0.45-ml cuvette as a function of coefficient values measured in infinite-medium geometry; the corresponding measured absorption coefficients are reported in (b). Values obtained in the small-volume cuvette setup include IL 1%, IL 2% (two samples), and IL 4%. In both (a) and (b), a line is drawn as a guideline to illustrate what would be a perfect 1:1 correspondence between small-volume and infinite-medium values.

times the transport mean free path.[8] In our setup, because the radius of the spherical chamber is approximately 5 mm, we wanted to bring the reduced scattering coefficient of the samples to a minimal value of 1 mm^{-1} or as close to it as possible. Optical properties measured on the cells plus beads solution are compared with those of the beads-only solution with the exact same concentration of beads. The difference in properties between the two samples corresponds to the cell contribution [Eq. (20)].

Cells that were the object of our investigations featured a spherical shape while in suspension. To confirm size changes in response to hypertonic conditions, we measured the mean cell diameter using a conventional phase-contrast microscope equipped with a 100×, 1.3-N.A. Ph 3 (phase 3) objective lens (Zeiss, Neofluar); cooled TE CCD acquisition hardware (Princeton Instruments); and digital image processing (IP Labs Spectrum, Scanalytics Inc., Fairfax, Va.). Typically, observations of up to ten independent fields of approximately ten cells (~100 cells) were used to determine the mean cell diameter.

3. Results

The possibility to enhance the photon path length in the small-volume cuvette is illustrated when we compare the theoretical functions describing PDW phase shift and amplitude to the infinite-medium geometry case (Fig. 2). Intuitively, an increase in phase shift corresponds to photons collected after a higher number of scattering events. We show here that use of a high-reflectance material ($R_{\text{eff}} > 95\%$) contributes to an increase in phase shift (and therefore path length) compared with the infinite-medium geometry at modulation frequencies greater than 150 MHz [Fig. 2(a)]. The amplitude versus frequency curve [Fig. 2(b)] shows that the signal level is improved with high-reflectivity cuvette walls, which reinforces the idea that PDW confinement can enhance measurement sensitivity (versus infinite media).

Figure 2 also underscores the important role played by the metal reflectivity on the PDW phase velocity behavior with respect to frequency. When the effective reflection coefficient R_{eff} remains close to 1, the phase shift versus frequency curve is highly nonlinear, affording optimal precision in the nonlinear fitting algorithm used to derive optical properties. Indeed, in this case the lower threshold to reach the dispersion regime for PDW propagation is close to the infinite-medium case. Reduction of the effective reflection coefficient to 75% introduces a loss mechanism. This extends the nondispersive, linear PDW

Table 1. Optical Properties of IL Solutions at 674, 811, and 849 nm

Sample	Literature μ_s'[a] (mm^{-1})	Infinite μ_s'[b] (mm^{-1})	Cuvette μ_s'[c] (mm^{-1})	Literature μ_a[d] (10^{-3} mm^{-1})	Infinite μ_a (10^{-3} mm^{-1})	Cuvette μ_a (10^{-3} mm^{-1})
674 nm						
IL 1%	1.2	1.14	1.05 ± 0.05	0.42	0.56	0.86 ± 0.16
IL 2%	2.4	2.17	2.12 ± 0.05	0.42	0.26	0.17 ± 0.14
IL 4%	4.8	NA[e]	4.16 ± 0.07	0.42	NA	0.92 ± 0.16
811 nm						
IL 1%	0.98	0.96	1.04 ± 0.06	2.32	2.30	2.11 ± 0.27
IL 2%	1.96	1.96	1.92 ± 0.08	2.32	2.54	2.46 ± 0.30
IL 4%	3.92	NA	3.66 ± 0.10	2.32	NA	2.97 ± 0.31
849 nm						
IL 1%	0.93	0.89	0.94 ± 0.06	4.33	3.64	2.97 ± 0.28
IL 2%	1.86	1.84	1.81 ± 0.07	4.33	3.57	3.91 ± 0.30
IL 4%	3.72	NA	3.61 ± 0.08	4.33	NA	4.56 ± 0.29

[a]Values obtained from Ref. 23.
[b]Values measured in infinite-medium geometry.
[c]Values obtained from small-volume cuvette experiments.
[d]Values obtained from Ref. 24.
[e]Not available.

regime to higher frequencies, decreases amplitude, and degrades nonlinear model fitting efficiency.[13]

We achieved experimental verification of our model by measuring the optical properties of well-described turbid solutions: three different concentrations of IL (1%, 2%, and 4%) were used to simulate scattering changes.[23] The phase shift is expected to increase along with increased values of μ_s', a behavior that is evidenced in Fig. 3(a), as is the decrease of amplitude of the signal over the frequency range [Fig. 3(b)]. Phase shift and ac amplitude versus frequency curves recorded experimentally were fit to model functions to extract the optical properties of the samples with the fitting strategy defined in Subsection 2.C.2.

The measurements on scattering phantoms were conducted at three different wavelengths (674, 811, and 849 nm) on the three different IL solutions; at each wavelength, one of the samples (IL 2%) was measured twice to check for process repeatability. Figure 4 displays a summary of the optical property results obtained when simultaneous fits were used for both phase and amplitude versus frequency curves. In Fig. 4(a), we show the values of the reduced scattering coefficient of IL solutions at three wavelengths versus values obtained from measurements performed in infinite-medium geometry, which are defined here as standard for our set of small-volume cuvette measurements. These values, when compared with those in the literature (see Table 1), give us an indication of the accuracy in the preparation of the solutions and FDPM experimental limitations. Figure 4(b) displays the absorption coefficients measured at the three wavelengths versus measurements performed in infinite-medium geometry, showing values stretching over one decade between 674 and 849 nm ($0.42–4.33 \times 10^{-3}$ mm^{-1}). The optical property values generated from the small-volume cuvette experiments are reported in Table 1, where they are compared with literature values for IL scattering[23] and water absorption[24] and with the standard values derived from infinite-medium experiments.

The effect of an added absorber to a scattering solution is not only to attenuate the amplitude, but it also reduces the phase lag because of the increased absorption of multiply scattered photons. Figure 5 displays the optical properties of IL 2% solutions with an absorber [i.e., NiSPC, which has an absorption peak close to 660 nm (Ref. 25)] added in increased concentrations (1, 2, and 4 μg/ml). The absorption coefficient of NiSPC was calibrated with a spectrophotometer (Beckman Instruments, Model DU-7): μ_a is equal to $0.81 \pm 0.02 \times 10^{-2}$ mm^{-1} for a concentration of 1 μg/ml of NiSPC at $\lambda = 674$ nm. In Fig. 5 the optical properties derived from the small-volume cuvette experiments are compared with the

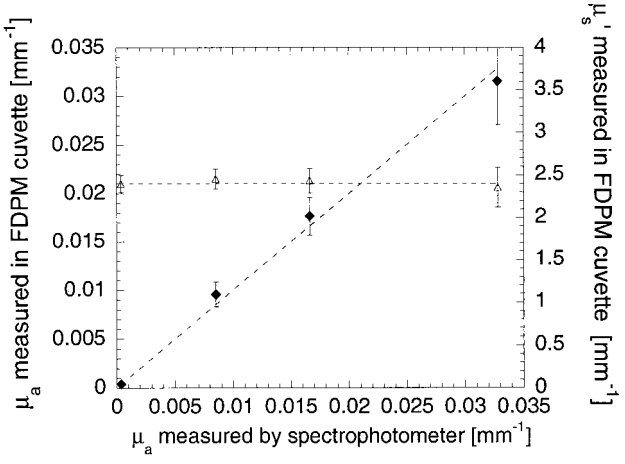

Fig. 5. Reduced scattering (triangles) and absorption (filled diamonds) coefficients of IL 2% solutions with NiSPC in different concentrations (0, 1, 2, and 4 μg/ml), measured in the small-volume cuvette setup at 674 nm. The dashed line shows the IL 2% calibrated value for μ_s' and the 1:1 correspondence between measured μ_a and μ_a calibrated with the spectrophotometer.

Table 2. Optical Properties of IL Solutions with NiSPC in Different Concentrations at 674 nm

Sample	Literature μ_s'[a] (mm^{-1})	Cuvette μ_s'[b] (mm^{-1})	Calibrated μ_a[c] (10^{-3} mm^{-1})	Cuvette μ_a (10^{-3} mm^{-1})
IL 2%	2.40	NA[d]	0.42	NA
IL 2% plus NiSPC 1 μg/ml	2.40	2.46 ± 0.11	8.52	9.54 ± 1.25
IL 2% plus NiSPC 2 μg/ml	2.40	2.43 ± 0.14	16.62	17.64 ± 1.95
IL 2% plus NiSPC 4 μg/ml	2.40	2.36 ± 0.23	32.82	31.52 ± 4.46

[a]Values obtained from Ref. 23.
[b]Values obtained from small-volume cuvette experiments.
[c]Values obtained from calibration of NiSPC absorption with a spectrophotometer; water absorption values are from Ref. 24.
[d]Not available.

calibrated values for the absorption and referenced to the calibration phantom (IL 2% without an absorber). The results show that μ_a values are linear with the absorber concentration and an added absorber does not affect the reduced scattering coefficient μ_s'. The optical property values are listed in Table 2, where they are compared with calibrated values for IL scattering and NiSPC absorption coefficients measured on pure solutions in the spectrophotometer.

Table 3 provides a comprehensive list of optical properties of microsphere suspensions measured in the small-volume cuvette compared with μ_s' values obtained from Mie theory[21] and μ_a values taken from the literature.[24] The comparison shows reasonably good agreement between experiment and theory for the reduced scattering coefficient (see also Fig. 6). In most cases, experimental values overestimate Mie predictions, with discrepancies ranging from 3% to 17% at 674 nm, 6.5% to 28% at 811 nm, and 1% to 8% at 849 nm. The absorption coefficients that we measured generally show a systematic overestimation at 674 and 811 nm and are comprised within 25% of the literature values at 849 nm.

The potential of our FDPM system to optically monitor cell physiological activity is illustrated in Fig. 7. Following the procedure described in Subsection 2.C.5, the optical properties of cells plus beads and beads-only suspensions were measured in the

Table 3. Optical Properties of Microsphere Solutions at 674, 811, and 849 nm

Sample	Mie μ_s'[a] (mm^{-1})	Cuvette μ_s'[b] (mm^{-1})	Literature μ_a[c] (10^{-3} mm^{-1})	Cuvette μ_a (10^{-3} mm^{-1})
674 nm				
0.698-μm beads (2.69%)	9.41	10.41 ± 0.07	0.42	1.93 ± 0.07
1.072-μm beads (2.68%)	7.74	8.60 ± 0.07	0.42	1.87 ± 0.08
1.531-μm beads (2.61%)	6.20	6.48 ± 0.08	0.42	1.12 ± 0.13
2.092-μm beads (2.61%)	5.04	5.91 ± 0.06	0.42	2.34 ± 0.11
2.092-μm beads (1.30%)	2.52	2.28 ± 0.05	0.42	0.15 ± 0.11
Mix 1[d]	6.84	7.04 ± 0.07	0.42	1.37 ± 0.09
Mix 2[e]	8.34	8.95 ± 0.07	0.42	1.65 ± 0.08
811 nm				
0.698-μm beads (2.69%)	8.06	8.75 ± 0.12	2.32	3.39 ± 0.19
1.072-μm beads (2.68%)	7.11	7.57 ± 0.12	2.32	3.57 ± 0.22
1.531-μm beads (2.61%)	5.67	6.20 ± 0.17	2.32	4.23 ± 0.38
2.092-μm beads (2.61%)	4.78	5.22 ± 0.11	2.32	4.12 ± 0.28
2.092-μm beads (1.30%)	2.39	3.06 ± 0.10	2.32	5.79 ± 0.37
Mix 1	6.33	7.44 ± 0.13	2.32	5.55 ± 0.27
Mix 2	7.26	8.76 ± 0.14	2.32	5.09 ± 0.24
849 nm				
0.698-μm beads (2.69%)	7.70	7.66 ± 0.09	4.33	3.55 ± 0.17
1.072-μm beads (2.68%)	6.78	6.70 ± 0.09	4.33	3.95 ± 0.19
1.531-μm beads (2.61%)	5.49	5.57 ± 0.09	4.33	3.54 ± 0.22
2.092-μm beads (2.61%)	4.61	4.99 ± 0.08	4.33	4.97 ± 0.23
2.092-μm beads (1.30%)	2.31	2.49 ± 0.07	4.33	4.83 ± 0.27
Mix 1	6.06	5.99 ± 0.08	4.33	3.86 ± 0.19
Mix 2	6.97	7.07 ± 0.06	4.33	3.25 ± 0.17

[a]Values obtained from Mie theory.[21]
[b]Values obtained from small-volume cuvette experiments.
[c]Values obtained from Ref. 24.
[d]66.67% of 1.072-μm beads plus 33.33% of 2.092-μm beads.
[e]66.67% of 0.698-μm beads plus 33.33% of 1.531-μm beads.

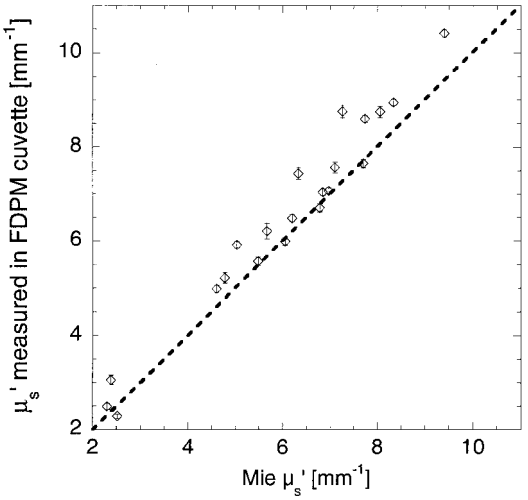

Fig. 6. Comparison between μ_s' values measured experimentally in the cuvette setup with values obtained from Mie theory. The samples are suspensions of microspheres of different sizes at three different wavelengths (674, 811, and 849 nm).

small cuvette. The cells used for these experiments were MCF7's. Salt was then added to the cells plus beads solution to reach a 2% saline level. Under these conditions, osmotic pressure induces cell shrinkage, which in turn translates into a scattering change (Table 4). This is portrayed best by a phase-shift decrease for the measurement on the cells plus beads solution when we go from isotonic to hypertonic conditions (triangles to squares in Fig. 7). The diameter of MCF7 cells, measured to be 18.7 ± 2.9 μm by video microscopy, decreases by 30% to 13.1 ± 2.1 μm in a 2% saline environment.

4. Discussion

Simulation results show that, for highly turbid samples, path-length enhancement can occur provided that the cuvette wall reflectance is 90% or higher. In fact, for $R_{\text{eff}} \approx 0.95$, multiple cuvette wall reflections contribute to additional PDW phase delay at high frequencies, improving the accuracy of optical property estimates from nonlinear model fits. In practical terms, this phenomenon introduces nonlinearity in the frequency-dependent PDW propagation. Consequently, all experiments were conducted in a 0.45-ml cuvette fabricated with silver surface deposition to achieve R_{eff} values of approximately 0.9.

The analysis of results displayed in Fig. 3 confirms that our relatively simple analytical model, based on a spherical geometry and radiative boundary, correctly describes experimental data. Both phase and

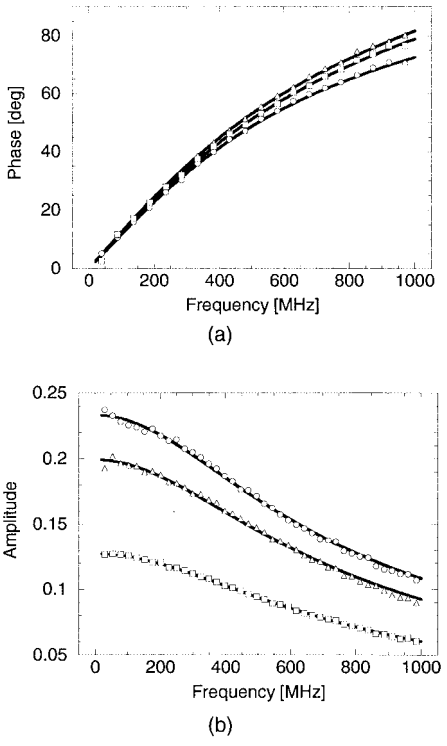

Fig. 7. (a) Phase shift and (b) amplitude measurements on MCF7 cell suspensions (0.75×10^8/ml) in the small-volume cuvette setup at 674 nm; the curves with circles indicate the beads-only suspension, triangles and squares refer to the beads plus cells suspension in isotonic and hypertonic environments, respectively.

amplitude analytical expressions fit remarkably well to the experimental recordings at the three different concentrations of IL solutions. Accurate values of the reduced scattering coefficient can be calculated from fits at all wavelengths [Fig. 4(a)]. The μ_s' estimation errors range from 2% to 6.5% of the true values. Absorption coefficients are also in good agreement with literature values. For 811- and 849-nm wavelengths, discrepancies between standards are, in all but one case (IL 1% at 849 nm), within the uncertainty of the measurements, ranging from 5% to 12%. The precision in the determination of small absorption coefficients, like water at 674 nm, is more difficult and inaccurate; however, these problems are not intrinsic to the small-cuvette system and can be encountered in infinite and semi-infinite geometry as well.[19] In this case, the mean absorption length is approximately 500 times greater than the cuvette radius, which explains why it is a challenge to obtain an accurate measurement.

Table 4. Optical Properties of MCF7 Cells in Isotonic and Hypertonic (saline 2%) Environments

Wavelength (μm)	μ_s' Isotonic (mm^{-1})	μ_s' Hypertonic (mm^{-1})	μ_s' Ratio	μ_a Isotonic (10^{-3} mm^{-1})	μ_a Hypertonic (10^{-3} mm^{-1})
0.674	0.935 ± 0.07	0.465 ± 0.07	0.497 ± 0.112	1.154 ± 0.126	1.406 ± 0.138
0.811	0.631 ± 0.128	0.343 ± 0.137	0.544 ± 0.327	3.209 ± 0.369	2.664 ± 0.406
0.849	0.586 ± 0.095	0.565 ± 0.097	0.964 ± 0.322	3.678 ± 0.313	3.802 ± 0.323

In Table 2 we observe that the experimental errors resulting from measurements of IL plus the NiSPC absorber range from 5% to 10% for μ_s' and 11% to 14% for μ_a. Errors increase at high absorber concentration, because PDW dispersion is delayed to higher frequencies.[13] As a result, the frequency dependence of phase and amplitude becomes more linear and more difficult to fit to nonlinear models. Overall, these measurements demonstrate our ability to accurately detect as little as a few hundred nanograms of absorber. This has important implications both for biochemical assays and for the detection of tissue inhomogeneities such as tumors and hemorrhagic lesions.

Measurement errors are primarily related to FDPM device features. These uncertainties have been discussed extensively in previous papers.[18,19] Additional errors unique to these experiments may be related to our inability to precisely place the APD detector at the surface of the spherical cuvette. This practical limitation should vanish because all sample measurements are performed relative to a reference at the beginning of each experimental session. However, a phase shift of 1.2 deg for a 1-mm distance in air at 1 GHz is an indication of its possible relevance.

Experiments conducted to observe light scattering by biological cells have been reported in the literature. In particular, Beauvoit *et al*.[26–28] concluded from their measurements that cell scattering was strongly correlated to the cell mitochondrial content and, interestingly, found that scattering was not influenced by the cell nucleus. Later, Mourant *et al*.[29] showed that the scattering coefficient of cell suspensions was mostly governed by the cell internal organelle structure. According to that study, the bigger structure of the cell, such as its external membrane, is reflected mainly in the anisotropy factor g. Other publications present theoretical models predicting cell scattering as a function of refractive-index structure and particle size distribution[30] or by use of a finite-difference model directly based on Maxwell's equations.[31]

The experiments reported in these publications required large volumes of cell solutions with, in some cases, complex experimental computational demands. Our FDPM cuvette demonstrates the possibility to use a simple, fast, single-measurement setup to determine the optical properties of small volumes of cell suspensions (0.45 ml), including the monitoring of changes in cell physiology under osmotic pressure (Table 4). Interpretation of these measured scattering changes in the context of contributions from subcellular structures may require application of complex models such as those used in the papers referenced above.[29–31]

5. Conclusion

We presented both theory and experimental verification of PDW propagation in a small-volume spherical geometry. A 0.45-ml reflective metallic cuvette was specially designed to test the model and analyze cell suspensions of optical properties. The theoretical model leads to relatively simple analytical expressions for frequency-dependent PDW dispersion. Under conditions of high cuvette reflectivity, substantial PDW path-length enhancement is observed. Optical property measurements for calibrated phantoms demonstrate that reduced scattering and absorption coefficients can be derived with accuracies of ~5–10% and ~10–15%, respectively, for scattering and absorption. Experiments on microsphere suspensions yield results consistent with Mie theory predictions and a systematic 5–10% overestimation of μ_s'. In dynamic measurements of cell suspensions, μ_s' tracks changes in cell dimension during osmotic challenge. Small-volume reflective cuvettes, combined with quantitative FDPM spectroscopy, may provide important new opportunities to analyze the optical properties and chemical composition of a broad variety of turbid samples.

This research was supported by the National Institutes of Health (NIH) Laser Microbeam and Medical Program and Optical Biology facilities (grants RR-01192 and CA-62203, respectively), NIH grant GM50958, the Whitaker Foundation (WF 16493), and Beckman Instruments Inc., Beckman Laser Institute programmatic support was provided by the U.S. Department of Energy (DOE DE-FG03-91ER61227) and the U.S. Office of Naval Research (ONR N00014-91-C-0134). O. Coquoz acknowledges the support of the Swiss National Science Foundation and Cancer Research Switzerland (BIL KFS 205-9-1995). The authors acknowledge C.-H. Sun and M. Booth for their outstanding contribution in preparing cell suspensions for our experiments and T. Krasieva for letting us benefit from her expertise in microscopy.

References

1. W.-F. Cheong, S. A. Prahl, and A. J. Welch, "A review of the optical properties of biological tissues," IEEE J. Quantum Electron. **26,** 2166–2185 (1990).
2. R. Marchesini, A. Bertoni, S. Andreola, E. Melloni, and A. E. Sichirollo, "Extinction and absorption coefficients and scattering phase functions of human tissues *in vitro*," Appl. Opt. **28,** 2318–2324 (1989).
3. V. G. Peters, D. R. Wyman, M. S. Patterson, and G. L. Frank, "Optical properties of normal and diseased human breast tissues in the visible and near infrared," Phys. Med. Biol. **35,** 1317–1334 (1990).
4. P. van der Zee, M. Essenpreis, and D. T. Delpy, "Optical properties of brain tissue," in *Photon Migration and Imaging in Random Media and Tissues*, R. R. Alfano and B. Chance, eds., Proc. SPIE **1888,** 454–465 (1993).
5. J. W. Pickering, S. A. Prahl, N. van Wieringen, J. F. Beek, J. C. Sterenborg, and M. J. C. van Gemert, "Double-integrating-sphere system for measuring the optical properties of tissue," Appl. Opt. **32,** 399–410 (1993).
6. H. Liu, M. Miwa, B. Beauvoit, N. G. Wang, and B. Chance, "Characterization of absorption and scattering properties of small-volume biological samples using time-resolved spectroscopy," Anal. Biochem. **213,** 378–385 (1993).
7. M. S. Patterson, B. Chance, and B. C. Wilson, "Time-resolved reflectance and transmittance for the noninvasive measure-

ment of tissue optical properties," Appl. Opt. **28,** 2331–2336 (1989).
8. P. Marquet, F. Bevilacqua, C. Depeursinge, and E. B. de Haller, "Determination of reduced scattering and absorption coefficients by a single charge-coupled device array measurement. I. Comparison between experiments and simulations," Opt. Eng. **34,** 2055–2063 (1995).
9. F. Bevilacqua, P. Marquet, C. Depeursinge, and E. B. de Haller, "Determination of reduced scattering and absorption coefficients by a single charge-coupled device array measurement. Part II: Measurements on biological tissues," Opt. Eng. **34,** 2064–2069 (1995).
10. T. J. Farrell, M. S. Patterson, and B. C. Wilson, "A diffusion theory model of spatially resolved, steady-state diffuse reflectance for the noninvasive determination of tissue optical properties *in vivo*," Med. Phys. **19,** 879–888 (1992).
11. J. B. Fishkin, O. Coquoz, E. R. Anderson, M. Brenner, and B. J. Tromberg, "Frequency-domain photon migration measurements of normal and malignant tissue optical properties in a human subject," Appl. Opt. **36,** 10–20 (1997).
12. B. J. Tromberg, O. Coquoz, J. B. Fishkin, T. Pham, E. R. Anderson, J. Butler, M. Cahn, J. Gross, V. Venugopalan, and D. Pham, "Non-invasive measurements of breast tissue optical properties using frequency-domain photon migration," Philos. Trans. R. Soc. London Ser. B **352,** 661–668 (1997).
13. B. J. Tromberg, L. O. Svaasand, T.-T. Tsay, and R. C. Haskell, "Properties of photon density waves in multiple-scattering media," Appl. Opt. **32,** 607–616 (1993).
14. J. B. Fishkin and E. Gratton, "Propagation of photon-density waves in strongly scattering media containing an absorbing semi-infinite plane bounded by a straight edge," J. Opt. Soc. Am. A **10,** 127–140 (1993).
15. J. R. Lakowicz and K. W. Berndt, "Frequency-domain measurements of photon migration in tissues," Chem. Phys. Lett. **166,** 246–252 (1990).
16. M. S. Patterson, J. D. Moulton, B. C. Wilson, K. W. Berndt, and J. R. Lakowicz, "Frequency-domain reflectance for the determination of the scattering and absorption properties of tissue," Appl. Opt. **30,** 4474–4476 (1991).
17. R. C. Haskell, L. O. Svaasand, T.-T. Tsay, T.-C. Feng, M. S. McAdams, and B. J. Tromberg, "Boundary conditions for the diffusion equation in radiative transfer," J. Opt. Soc. Am. A **11,** 2727–2741 (1994).
18. S. J. Madsen, R. C. Haskell, and B. J. Tromberg, "A portable, high-bandwidth frequency-domain photon migration instrument for tissue spectroscopy," Opt. Lett. **19,** 1934–1936 (1994).
19. T. H. Pham, O. Coquoz, J. B. Fishkin, E. Anderson, and B. J. Tromberg, "Broad bandwidth frequency domain instrument for quantitative tissue optical spectroscopy," Rev. Sci. Instrum. **71,** 2500–2513 (2000).
20. W. H. Press, S. A. Teukolsky, W. T. Vetterling, and B. D. Flannery, *Numerical Recipes in C: The Art of Scientific Computing* (Cambridge U. Press, Cambridge, UK, 1992).
21. C. F. Bohren and D. R. Huffman, *Absorption and Scattering of Light by Small Particles* (Wiley, New York, 1983).
22. B. Gelebart, E. Tinet, J.-M. Tualle, and S. Avrillier, "Phase function simulation in tissue phantoms: a fractal approach," Pure Appl. Opt. **5,** 377–388 (1996).
23. H. J. van Staveren, C. J. M. Moes, J. van Marle, S. A. Prahl, and M. J. C. van Gemert, "Light scattering in Intralipid-10% in the wavelength range of 400–1100 nm," Appl. Opt. **30,** 4507–4514 (1991).
24. G. M. Hale and M. R. Querry, "Optical constants of water in the 200-nm to 200-μm wavelength region," Appl. Opt. **12,** 555–563 (1973).
25. B. J. Tromberg, R. C. Haskell, S. J. Madsen, and L. O. Svaasand, "Characterization of tissue optical properties using photon density waves," Comments Mol. Cell Biophys. **8,** 359–386 (1995).
26. B. Beauvoit, H. Liu, K. Kang, P. D. Kaplan, M. Miwa, and B. Chance, "Characterization of absorption and scattering properties of various yeast strains by time-resolved spectroscopy," Cell Biophys. **23,** 91–109 (1993).
27. B. Beauvoit, K. Kitai, and B. Chance, "Contribution of the mitochondrial compartment to the optical properties of rat liver: a theoretical and practical approach," Biophys. J. **67,** 2501–2510 (1994).
28. B. Beauvoit, S. M. Evans, Y. W. Jenkins, E. Miller, and B. Chance, "Correlation between the light scattering and the mitochondrial content of normal tissues and transplantable rodent tumors," Anal. Biochem. **226,** 167–174 (1995).
29. J. R. Mourant, J. P. Freyer, A. H. Hielscher, A. A. Eick, D. Shen, and T. M. Johnson, "Mechanisms of light scattering from biological cells relevant to noninvasive optical-tissue diagnostics," Appl. Opt. **37,** 3586–3593 (1998).
30. J. Schmitt and G. Kumar, "Optical scattering properties of soft tissue: a discrete particle model," Appl. Opt. **37,** 2788–2797 (1998).
31. A. Dunn and R. Richards-Kortum, "Three-dimensional computation of light scattering from cells," IEEE J. Sel. Top. Quantum Electron. **2,** 898–905 (1996).